Available online at www.sciencedirect.com

ScienceDirect

journal homepage: www.elsevier.com/locate/he

ReaxFF molecular dynamics simulation of nickel catalysed gasification of cellulose in supercritical water

*Mengwei Yu, Cheng Chen, Zhihao Xing, Xi Jiang**

School of Engineering and Materials Science, Queen Mary University of London, Mile End Road, London E1 4NS, UK

HIGHLIGHTS

- The H atoms in cellulose are the primary source of H_2 production.
- Reducing the concentration of hydroxyl radical is beneficial to H_2 yield.
- The deoxygenation and dehydroxylation of cellulose on Ni surface decrease the CO yield.
- Water would occupy the Ni active sites and prevent the adsorption of organic fragments.
- High temperature enables carbon to permeate into the interior region of the catalyst.

GRAPHICAL ABSTRACT

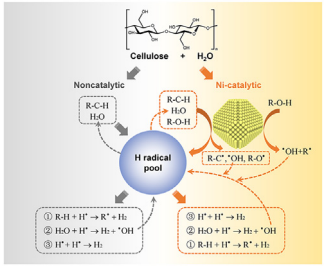

ARTICLE INFO

Article history:
Received 20 July 2022
Received in revised form
19 September 2022
Accepted 21 September 2022
Available online 14 October 2022

Keywords:
Cellulose
Catalytic gasification
Supercritical water
Reactive molecular dynamics

ABSTRACT

Reactive force field (ReaxFF) molecular dynamic simulation was performed to elucidate the mechanism of Ni-catalysed supercritical water gasification of cellulose considering the effects of temperature and cellulose to water ratio. Simulations showed that Ni could decrease the activation energy of C–C and C–O bond cleavage, promoting the depolymerisation and ring-opening process of cellulose. The yields of gaseous products increase with the increasing temperature. H_2 yield mainly depends on H free radical number, which can be generated from cellulose dehydrogenation and water splitting reactions. These two reactions were promoted on Ni surface, leading to an increase in H_2 yield. In the presence of Ni catalyst, water plays a limited role in providing H free radicals to produce H_2, while the hydrogen atoms in cellulose are the primary source of H_2 generation. Meanwhile, reducing the concentration of $^{\bullet}OH$ could enhance H_2 production as the combination of $^{\bullet}OH$ and $H^{\bullet}$ is a H radical consumption process. Small organic fragments would be absorbed on the Ni surface, where they undergo deoxygenation via the cleavage of C–O bonds, resulting in a decrease in CO and CO_2 yields. The increase in water mass fraction would promote the H_2 yield as more H radical would be produced due to water splitting reaction. Moreover, the addition of water would occupy the Ni active sites and prevent the adsorption of organic

* *Corresponding author.*
E-mail address: xi.jiang@qmul.ac.uk (X. Jiang).

https://doi.org/10.1016/j.ijhydene.2022.09.202

fragments. These dissociative fragments are prone to produce more CO. The carbon deposition on the Ni surface results in the deactivation of the catalyst. Simulation results suggested that carbon deposition and permeation increase with increasing temperature. In contrast, the increase in water mass fraction can favour carbon elimination from the catalyst surface.

Introduction

Biomass is an effective energy carrier, contributing to the growing demand for clean and everlasting energy sources for the sustainable development of society. Biomass can be converted to biofuel through biochemical technologies (e.g., fermentation and anaerobic digestion) and thermochemical technologies (e.g., pyrolysis, liquefaction, gasification and torrefaction) [1]. One of the leading technical barriers to industrialising biomass-derived energy is the high energy input of conversion processes, especially for biomass with high moisture content. Wet bio-feedstocks require energy-costly drying operation, reducing the efficiency of the energy conversion process. However, supercritical water gasification (SCWG) technology may overcome this problem as the wet biomass can be directly gasified without an energy-intensive drying step. For high moisture biomass, the energy required for the drying process is higher than that of heating the water to a supercritical point. It was reported that the total efficiency of heat utilisation of biomass SCWG is higher than that of thermal gasification when the moisture content exceeds 27% [2]. SCWG of wet biomass can produce H_2-rich syngas, which has a high heating value and can be used as a cleaner alternative of fossil fuels.

Biomass gasification is a process that converts feedstock materials into gaseous products such as syngas at high temperature conditions (above 700 °C), with a controlled amount of oxygen and/or steam but without combustion. One of the primary benefits of SCWG technology is associated with the high-pressure/high-temperature water that is used as the reaction medium. The physical properties of water drastically change when the pressure/temperature conditions are above its critical point. As the reaction medium, supercritical water (SCW) offers several advantages, such as low viscosity, high diffusion coefficient, and complete miscibility with varying organics and gases, thereby enhancing the mass transfer and reaction rate in the reactor [1,3].

Cellulose is one of the main structural components of lignocellulose biomass, constituting 40–50 wt% of lignocellulosic biomass on a dry weight basis [4]. Moreover, it is reported that the contribution of cellulose to H_2 production during the gasification process is more than that of hemicellulose and lignin [5]. Therefore, it is essential to investigate the conversion mechanism of cellulose during the SCWG process. Extensive experimental studies on SCWG of cellulose have been carried out [1,3,6]. Cellulose comprises glucose monomers linked together by β-1,4 D-glucopyranose bonds, forming strong intramolecular and intermolecular hydrogen bonds [3]. Cellulose undergoes rapid hydrolysis and decomposes to its monomer (e.g., glucose) at very short residence times under elevated pressure/temperature. Then glucose undergoes hydrolysis to liquid-phase organic intermediates, followed by the slower formation of small quantities of stable light gases [7]. Therefore, cellulose is one of the most refractory substances that are difficult to dissolve in hot water [8], requiring harsh operating conditions to convert it into biofuel. It is widely accepted that a higher operating temperature favours the formation of H_2 [1,5]. However, heating the feedstock and water to supercritical conditions is an energy-consuming process. Lowering the reaction temperature of SCWG and improving the conversion efficiency are essential for promoting the commercial utilisation of SCWG.

The use of catalysts in SCWG is one of the most promising approaches to improve the gas yield while minimising the heat requirements, which can reduce the operating costs of the process [9]. Nickel-based catalyst is one of the most effective transition metal catalysts in biomass gasification for improving the gas yield and preventing the formation of tar (heavy hydrocarbons produced during SCWG, which can contaminate equipment and lead to increased maintenance costs) [10]. Extensive studies have been carried out to investigate the catalytic effect of Ni on the gaseous product yield in the biomass SCWG process [9,10]. It is widely accepted that Ni could effectively promote water gas shift reaction and steam reforming reaction [11,12], which are the two main reactions occurred in SCWG to produce hydrogen. Nickel (Ni) is known for its tendency to catalyse the cleavage of C–C, C–O, and O–H bonds [13,14], which promotes the formation of various carbonaceous products. The cracking products can be effectively dehydrogenated to produce more hydrogen [15]. Kumar and Reddy [16] investigated the impacts of Ni, Ru, and Fe on the gas yield during SCWG of banana pseudo-stem. The results showed that Ni has the highest activity in H_2 generation. Ruppert et al. [14] studied the thermochemical conversion of cellulose for hydrogen production with Ni/ZrO_2. They considered that the organic intermediates probably undergo dehydrogenation on the metal surface, hence increasing H_2 yield. The cleavage of C–C and C–O bonds can occur to form various carbonaceous products. However, the proposed mechanisms were primarily based on the analysis of products detected during the SCWG process. Detailed structural changes at the molecular level, such as radicals and intermediates in cellulose dissociation and steam reaction, can

hardly be captured through experimental methods. The exact mechanism of Ni catalytic thermal decomposition of cellulose has not been fully understood and further investigation is needed.

Molecular dynamics (MD) simulation provides an opportunity to investigate the underlying mechanisms of catalytic SCWG of biomass at an atomic level. MD with ReaxFF can simulate the cleavage and forming of chemical bonds to identify elementary pathways. ReaxFF MD simulations were adopted to study the SCWG of lignin [17–20]. The structural evolution of lignin and the chemical reactions of forming CO, CO_2, CH_4, and H_2 were obtained. Zhang et al. [21] conducted a molecular study on SCWG of glucose under microwave heating. They found that the external electric fields promote glucose decomposition to produce formaldehyde and hydrogen-free radicals, increasing H_2 yield. The ReaxFF approach has been successfully employed to study the SCWG of biomass catalysed by the metal catalyst. The work of Monti et al. [22] showed that the ReaxFF approach was able to obtain an atomic-level characterisation of the crucial steps of the adsorption of the lignin molecules on the Palladium catalyst, including their fragmentation and desorption. The SCWG of lignin with Pt and Ni nanoparticles was studied by using ReaxFF simulation [23]. It was found that the Pt and Ni reduce the degradation temperature, accelerating the aromatic ring-opening process. The ReaxFF simulation study of Fe-catalysed SCWG of lignin revealed that Fe iron with a low oxidation state contributes to the formation of CO, while iron with a high oxidation state was beneficial to increasing CO_2 yield [24]. The evolution of the lignin decomposition catalysed by Ni was investigated with ReaxFF simulation [25]. The results indicated that Ni could potentially accelerate the scission of C–O bonds and destroy the conjugated π bond of the aromatic ring during the ring-opening process. The generation process of H_2 molecules occurring on the Ni surface was presented. The thermal stability of carboxymethyl cellulose on the Fe_2O_3 surface was studied by Saha et al. [26]. It was found that cellulose can be adsorbed on the metal surface via the formation of bonds between Fe and oxygen atoms. The chemisorption would bulge the Fe slightly out of the Fe_2O_3 surface.

Although significant experimental work has been performed on Ni catalytic SCWG of biomass, there is a lack of detailed understanding on the chemical processes involved at the molecular level. Further fundamental modelling studies are required to deepen the understanding of the catalytic and micro reaction degradation mechanisms during the SCWG process. This could provide a basis for optimising operating conditions and developing high-efficiency catalysts, thereby promoting the utilisation of SCWG technology. To the best of our knowledge, the ReaxFF simulation of Ni catalysed SCWG of cellulose has not been carried out. This study investigated the effect of Ni on cellulose depolymerisation and ring-opening process. The effects of temperature and cellulose-to-water mass ratio (C/W) on gaseous products were investigated. The detailed gaseous product generation pathways were analysed. Besides, the influence of temperature and C/W on carbon deposition behaviour on Ni nanoparticle (NiNP) was investigated.

Modelling methodology

Computational method

All MD simulations in this work were conducted using the ReaxFF force field [27]. The description of connectivity-dependent interactions in the ReaxFF force field is based on bond order formalism. Bond order is determined by interatomic distance using an empirical formula, including contributions from σ, π and ππ bonds. The chemical reactions during the time intervals can be analysed based on the interatomic potential and the bond order. Nonbonded interactions, such as Coulomb and van der Waals interaction, are calculated independently. The charge equilibration (QEq) method adjusts the partial charge on individual atoms. The following equation calculates the energy of each particle:

$$Esystem = Ebond + Eover + Eunder + Elp + Eval + Etor + EvdWaals + Ecoulomb \quad (1)$$

where E_{bond}, E_{over}, E_{under}, E_{lp}, E_{val}, E_{tor}, $E_{vdWaals}$, and $E_{coulomb}$ stand for bond energy, overcoordination energy penalty, undercoordination stability, lone pair energy, three-body valence angle energy, four-body torsional angle energy, van der Waals energy, and Coulomb energy, respectively. In this study, the C/H/O/Ni parameter set [28,29] developed for modelling hydrocarbon chemistry catalysed by Ni was adopted to study the cellulose SCWG catalysed by Ni nanocatalysts. The verification of the adopted force field was carried out in our previous work [30].

Model construction and simulation setup procedures

Cellulose $(C_6H_{10}O_5)_n$ is a polysaccharide consisting of a linear chain of several hundred to many thousands of β-1,4 linked D-glucopyranose units. Fig. 1 shows the model used in the MD simulations. The model construction starts with a monomer, and the unimolecular D-glucopyranose was built and optimised using the Materials Studio [31] Forcite module. Ten D-glucopyranose monomers were connected to form a polymer, as shown in Fig. 1(c). Face-centred cubic lattice of NiNP was created on a web-based crystallographic tool [32]. The minimum surface energy of corresponding Miller indices of (111), (100) and (110) was adopted from the work of Chen et al. [30]. The melting temperature of NiNP depends on its size, and the melting temperature decreases with decreasing radius of NiNP. The melting temperature of 3 nm NiNP simulated with the ReaxFF force field is around 1700 K [30], which is lower than the simulation temperature (1800 K~2200 K) in this study. The simulated melting temperature of 4.0 nm NiNP is around 2000 K by using the same ReaxFF force field [30]. Although the 4.0 nm NiNP would melt to some degree when the temperature is above 2000K, the NiNP still keeps a spherical shape. Therefore, NiNP with a diameter of 4.0 nm was adopted to maintain the integrity of NiNP during the simulation in this study.

Eight reaction systems S1–S8 were built to investigate the Ni catalytic SCWG of cellulose, as listed in Table 1. Different cellulose molecule numbers have been tested to eliminate the effect of atom number on the simulation results. Ten cellulose

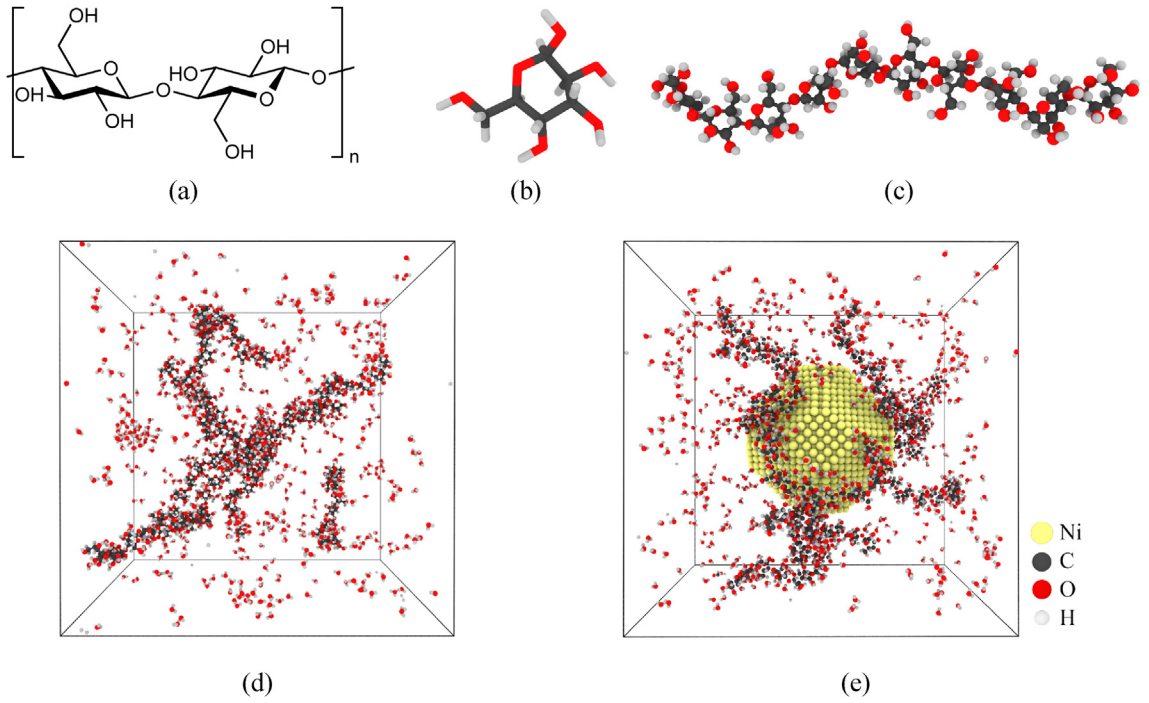

Fig. 1 – MD simulation model: (a) Structural formula of cellulose; (b) D-glucopyranose molecule; (c) Constructed cellulose structure with ten β-1,4 linked D-glucopyranose units; (d) Snapshot of noncatalytic SCWG of cellulose at 100 ps; (e) Snapshot of Ni catalytic SCWG of cellulose at 100 ps, where NiNP was fixed in the centre with water and cellulose molecules distributed around.

molecules were adopted to ensure the validity of simulation results. To observe the reactions that occur on the Ni surface, the catalyst to biomass ratio considered is relatively high. Cases S1–S6 are used to study the effects of temperature and catalyst on the SCWG of cellulose. Cases S5, S7, and S8 are used to study the effect of cellulose-to-water mass ratio (C/W) on the catalytic SCWG of cellulose. The system pressure would affect the yield of gaseous products. An increase in pressure will shift the methanation reactions ($CO + 3H_2 \leftrightarrow CH_4 + H_2O$, $CO_2 + 4H_2 \leftrightarrow CH_4 + 2H_2O$) to the right, thereby enhancing the formation of CH_4 [1]. Therefore, the simulation box dimensions were adjusted to keep the same pressure in systems S7 and S8 with varying water molecules.

Sorensen and Voter [33] pointed out that an elevated temperature could accelerate the reaction process and thus significantly extend the simulation time scale, which has become a familiar and effective strategy in ReaxFF MD simulation [24,34]. For reaction rates described by the Arrhenius equation, increasing the temperature would increase the reaction rates but not the activation energy barrier. Salmon et al. [35] studied coal pyrolysis using ReaxFF simulation at an elevated temperature. They compared the simulated product distribution with experimental results and concluded that elevated temperature did not influence the reaction pathways during coal pyrolysis. Accordingly, elevated reaction temperatures were chosen in this work to study the catalytic mechanism of Ni during the SCWG of cellulose.

Initial configurations of all models were built by using Packmol [36]. Cellulose and water molecules are distributed randomly into the cubic box, and the box dimensions are listed in Table 1. In catalytic SCWG (e.g., cases S4–S8), NiNP was fixed in the centre of the unit cell and water and cellulose molecules are distributed around, as shown in Fig. 1(e). After system energy minimisation, the simulation cell was relaxed at 300 K for 20 ps. Subsequently, the equilibrated system was heated to the final reaction temperature with a heating rate of

Table 1 – Detailed simulation cases for the studied systems of Ni catalytic SCWG of cellulose.

Cases	Cellulose molecules	Water molecules	C/W[a]	Catalyst	Temperature	Box dimensions (Å)
S1	10	600	3:2	–	1800 K	90 × 90 × 90
S2	10	600	3:2	–	2000 K	90 × 90 × 90
S3	10	600	3:2	–	2200 K	90 × 90 × 90
S4	10	600	3:2	NiNP	1800 K	90 × 90 × 90
S5	10	600	3:2	NiNP	2000 K	90 × 90 × 90
S6	10	600	3:2	NiNP	2200 K	90 × 90 × 90
S7	10	900	3:3	NiNP	2000 K	98 × 98 × 98
S8	10	300	3:1	NiNP	2000 K	85 × 85 × 85

[a] C/W is the cellulose-to-water mass ratio.

15 K/ps. Then, the simulations would last at the target temperature for 2 ns. All simulations were performed using an isochoric-isothermal NVT (fixed atom numbers, volume, and temperature) ensemble. A time step of 0.25 fs was assigned. The trajectories and species information were outputted every 100 steps. The linear and angular momentum of NiNP was zeroed every 10 timesteps.

The periodic boundary condition was applied in all directions. The initial velocities for all atoms were generated randomly following the Maxwell-Boltzmann distribution. Nosé-Hoover thermostat and barostat were adopted to control the system temperature and pressure with a temperature and pressure damping constant equal to 100 times and 1000 times of the time step, respectively. A bond order of 0.3 was employed to identify chemical bonds between pairs of atoms [28,30]. All simulations were repeated three times with different initial configurations and velocity distributions. The ReaxFF MD simulations were performed with the REAXC package [37] in the Large-scale Atomic/Molecular Massively Parallel Simulation (LAMMPS) [38].

Results and discussion

The effect of Ni on the depolymerisation and ring-opening process of cellulose

The first step in cellulose conversion involves its depolymerisation to oligomers or D-glucopyranose [4], which undergoes hydrolysis to form liquid-phase organic intermediates via scission of C–C and C–O bonds. Guo et al. [9] established the mechanism of Ru catalytic gasification of D-glucopyranose. Hydroxyl groups are adsorbed to the catalytic Ru surface predominantly through oxygen atoms. The reactant undergoes dehydrogenation on the catalyst surface, followed by subsequent cleavage of C–C or C–O bonds, which results in syngas production. However, the detailed adsorption and degradation process on catalyst surfaces are not readily accessible by experiments.

The depolymerisation and ring-opening percentage of cellulose during the heating period in cases S2 and S5 are shown in Fig. 2(a) and (b). The depolymerisation and ring-opening percentage are computed by the following equations:

$$\text{Depolymerisation percentage} = \frac{\text{Cleavage of } \beta-1,4 \text{ linkage}}{\text{Initial number of } \beta-1,4 \text{ linkage}} \times 100\left(\%\right) \quad (2)$$

$$\text{Ring}-\text{opening percentage} = \frac{\text{Number of opened ring}}{\text{Initial number of ring}} \times 100\ (\%) \quad (3)$$

It can be seen that Ni could accelerate the depolymerisation and ring-opening process of cellulose. The depolymerisation and ring-opening occur at around 75 ps in the absence of Ni catalyst, and almost all β-1,4 linkages are cracked after 125 ps. While the start points of β-1,4 linkage cleavage and ring-opening are around at 50 ps in the presence of Ni catalyst, these processes were completed after 100 ps. The results show that decomposition of cellulose can occur at a lower temperature, which helps reduce the cost of biomass SCWG. The two cases show a similar onset time and evolution trend in depolymerisation and ring-opening processes, demonstrating that the ring-opening takes place immediately after cellulose is depolymerised into monomers. This is because the cleavage of β-1,4 linkage would lead to the structural instability of the corresponding monomer, resulting in the ring-opening of D-glucopyranose.

The ring-opening of the D-glucopyranose monomer can be achieved by the cleavage of the C–C or C–O bond. Fig. 2(c) shows the cleavage percentage of different types of bonds. Around 64% of rings were opened by the cleavage of the C–O bond in the absence of Ni, while this figure increases to 70% when Ni was added. This result suggests that more rings of D-glucopyranose tend to be opened via the cleavage of the C–O bond under the effect of Ni catalyst.

Both high temperature and catalyst would promote bond breaking. The energy of atoms increases with increasing temperature, and the bonds between the atoms become more unstable and eventually break. Catalysts make this process more efficient by lowering the activation energy. If an atom forms a chemical bond with Ni atoms, the cleavage of other chemical bonds connected to this atom will take place. The cracking of such bonds is considered as catalytic cleavage and the others are considered as thermal cleavage. The thermal cleavage and catalytic cleavage of bonds during depolymerisation and ring-

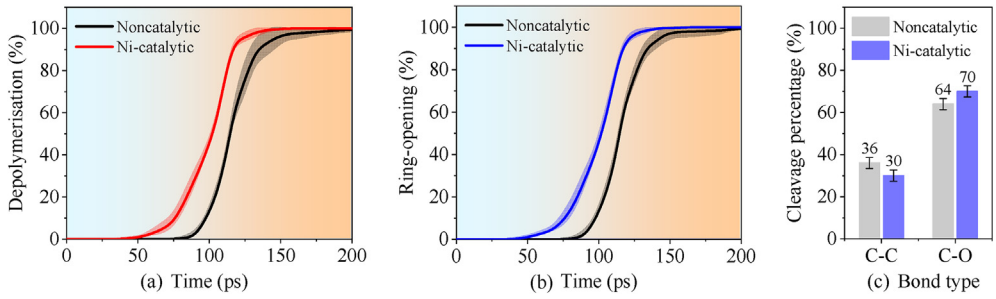

Fig. 2 – (a) The depolymerisation and (b) ring-opening percentage of cellulose during the heating period in cases S2 and S5, the colour gradient (from blue to red) in the background represents increasing temperature; (c) Cleavage percentage of C–C and C–O bonds during the ring-opening process in cases S2 and S5. (For interpretation of the references to color/colour in this figure legend, the reader is referred to the Web version of this article.)

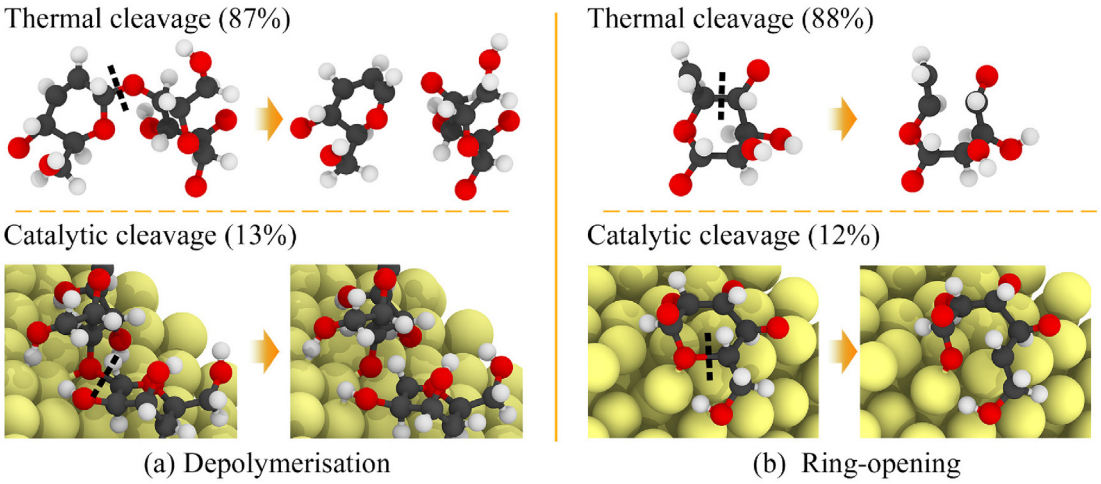

Fig. 3 – Thermal bond cleavage and catalytic bond cleavage during (a) depolymerisation and (b) ring-opening process in case S5. The percentage represents the proportion of two types of cleavage. Black dash lines represent the bond cleavage sites.

opening process in catalytic SCWG (case S5) are shown in Fig. 3. It can be seen that 87% and 88% of bond breakings take place via thermal cleavage during depolymerisation and ring-opening process, respectively. Thermal cleavage of bond plays a dominant role in the bond-breaking process. Therefore, depolymerisation and ring-opening rate in noncatalytic and catalytic SCWG are similar after 100 ps, when the temperature of the system reaches a certain value, as shown in Fig. 2.

As the skeleton of organic matters, the dissociation kinetics of C–C and C–O bonds play a vital role in cellulose decomposition. The decomposition reactions of D-glucopyranose were considered to be first-order reactions [39]. Initial and equilibrium numbers of C–C and C–O bonds can be used to calculate the activation energy of the corresponding bond [40,41]. The reaction rate constant, *K*, is determined by the following equation [40]:

$$\ln N_0 - \ln N_{teq} = Kt_{eq} \tag{4}$$

where N_0 and N_{teq} are the numbers of C–C or C–O bonds at initial and equilibrium stages. The reaction rates are analysed by the Arrhenius equation:

$$K = A\exp\left(-\frac{E_a}{RT}\right) \tag{5}$$

where R is the universal gas constant. The activation energy (Ea) and the pre-exponential factor (A) in Eq. (5) are calculated by linear fitting. Fig. 4 shows the change in the activation energy of C–C and C–O bonds in the absence and presence of a catalyst. The activation energy of the C–C bond is 25.33 kJ/mol without catalyst, and this figure decreases to 24.02 kJ/mol when Ni catalyst is added. Activation energies for C–O bonds without and with Ni are calculated as 24.95 and 22.97 kJ/mol, respectively. It can be seen that the activation energy of C–O bonds is lower than that of C–C bonds. Thereby, the ring-opening of D-glucopyranose monomers is prone to take place via the cleavage of C–O bonds. Moreover, the activation

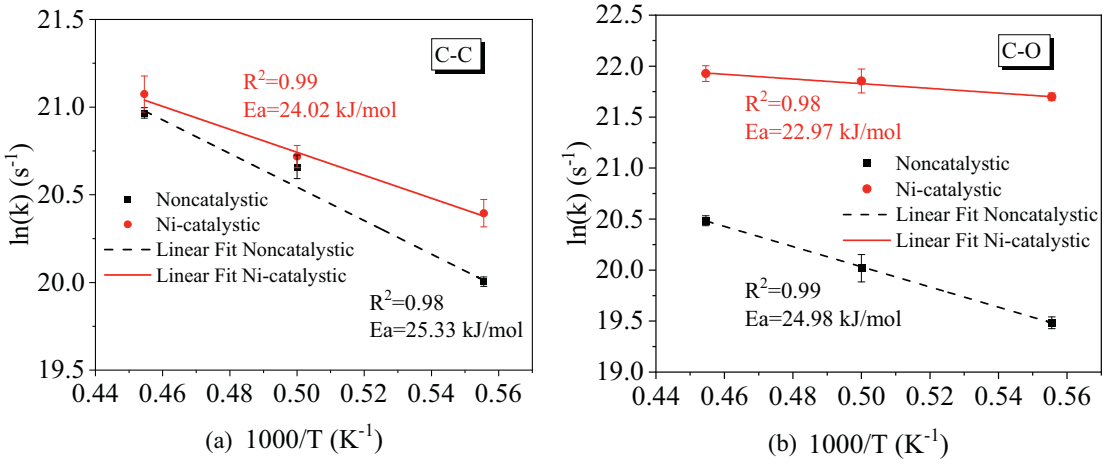

Fig. 4 – Temperature-dependent dissociation rates (k) of C–C and C–O bonds during the SCWG processes of cellulose (R^2 is the coefficient of determination).

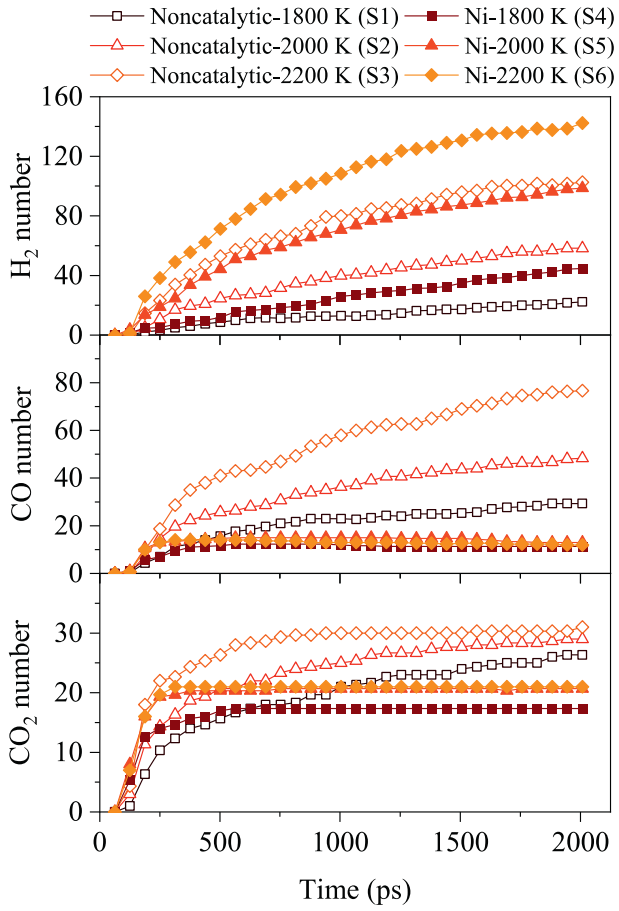

Fig. 5 – Time evolution of the total number of H_2, CO, and CO_2 molecules at different temperatures during SCWG of cellulose with and without Ni catalyst.

energy reduction of C–O bonds (1.98 kJ/mol) under the effect of catalyst is more significant than that of C–C bonds (1.31 kJ/mol), demonstrating Ni is more efficient in the cleavage of the C–O bond than the C–C bond. Consequently, the proportion of C–O cleavage increases when Ni is added during the ring-opening process, as shown in Fig. 2(c). It has been reported that cellulose is easier to gasify than lignin in the presence of Ni catalyst [42], which can be explained by the structural differences between cellulose and lignin because there are more C–O bonds in cellulose molecules than in lignin.

The effect of Ni on the gaseous product yield

Fig. 5 shows the time evolution of the total number of H_2, CO, and CO_2 molecules at different temperatures during SCWG of cellulose in the absence and presence of Ni catalyst. Temperature is one of the most dominant parameters that affect the gaseous product yield, especially when the reaction occurs without a catalyst [1]. Generally, the gaseous produce yield increases with an increase in reaction temperature as high temperatures favour the scission of C–C and C–O bonds. The simulation results show that H_2 yield increases with increasing temperature, which is consistent with the experimental results [43]. The free radical reactions in water are believed to be temperature-dependent. When the conditions are above the critical point of water, free radical reactions dominate over ionic reactions [3]. Therefore, water splitting at higher temperature generates more H free radicals. In addition to water splitting reaction, biomass dehydrogenation reaction would also be enhanced at high temperatures [44]. The increase of H free radical number leads to the increase in H_2 yield, which will be discussed subsequently.

Ni catalyst will significantly increase the yield of H_2, as shown in Fig. 5. The H_2 generation pathways were analysed to explore the effect of Ni on the H_2 production mechanism. The generation of H_2 is mainly through the following three pathways:

① $\text{R-H} + \text{H}^\bullet \rightarrow \text{R}^\bullet + \text{H}_2$
② $\text{H}_2\text{O} + \text{H}^\bullet \rightarrow \text{H}_2 + {}^\bullet\text{OH}$
③ $\text{H}^\bullet + \text{H}^\bullet \rightarrow \text{H}_2$

where pathway ①: hydrogen transfer reactions, where H radical interacts with the H atoms in cellulose to produce H_2 [17,45]; pathway ②: H radical interacts with water to produce H_2 and OH at elevated temperature [17,46]; pathway ③: H radical termination reaction, where two H radicals interact with each to produce H_2 [17,45]. R is the abbreviation for any other groups.

The occurrence frequency and proportion of pathways ①-③ during SCWG of cellulose in the absence and presence of Ni catalyst are presented in Fig. 6(a) and Fig. 6(b), respectively. The results suggest that pathway ① plays a dominant role in the H_2 generation in the absence of Ni catalyst, especially at relatively low temperatures. It can be seen that around 68% of H_2 was produced via pathway ① in 1800 K. Only a few H_2 molecules were generated through pathway ③ without Ni catalyst. However, pathway ③ becomes the main H_2 generation path with the addition of Ni catalyst. More than 70% of H_2 molecules were generated via pathway ③, and this figure reached 82% in 1800 K. This is because a large number of H free radicals would be generated by the water splitting and cellulose dehydrogenation reactions on the Ni surface. Increasing the concentration of H free radical enhances the occurrence frequency of pathway ③. Meanwhile, the frequency of all three pathways increases with increasing temperature, and the increase of pathway ② is the most significant. Therefore, the proportion of pathway ② increases with increasing reaction temperature, as shown in Fig. 6(b).

The yield of H_2 is closely related to the number of H free radicals. The generation paths of H free radicals were analysed to investigate the effect of Ni on H_2 yield. The H radicals could be produced from the water splitting and cellulose dehydrogenation reactions, as listed in the following pathways:

④ $\text{H}_2\text{O} \leftrightarrow {}^\bullet\text{OH} + \text{H}^\bullet$
⑤ $\text{R-O-H} \leftrightarrow \text{R-O}^\bullet + \text{H}^\bullet$
⑥ $\text{R-C-H} \leftrightarrow \text{R-C}^\bullet + \text{H}^\bullet$

where pathway ④: free radical reaction of water, where H_2O splits into $H^\bullet$ and $^\bullet OH$ or the radicals recombine into H_2O at elevated temperature [3]; pathway ⑤ and pathway ⑥: dehydrogenation reaction of cellulose, where the H atom connects to or disconnects from oxygen and carbon atoms respectively [41]. Due to the high activity of free radicals, the reaction pathways ④-⑥ are reversible.

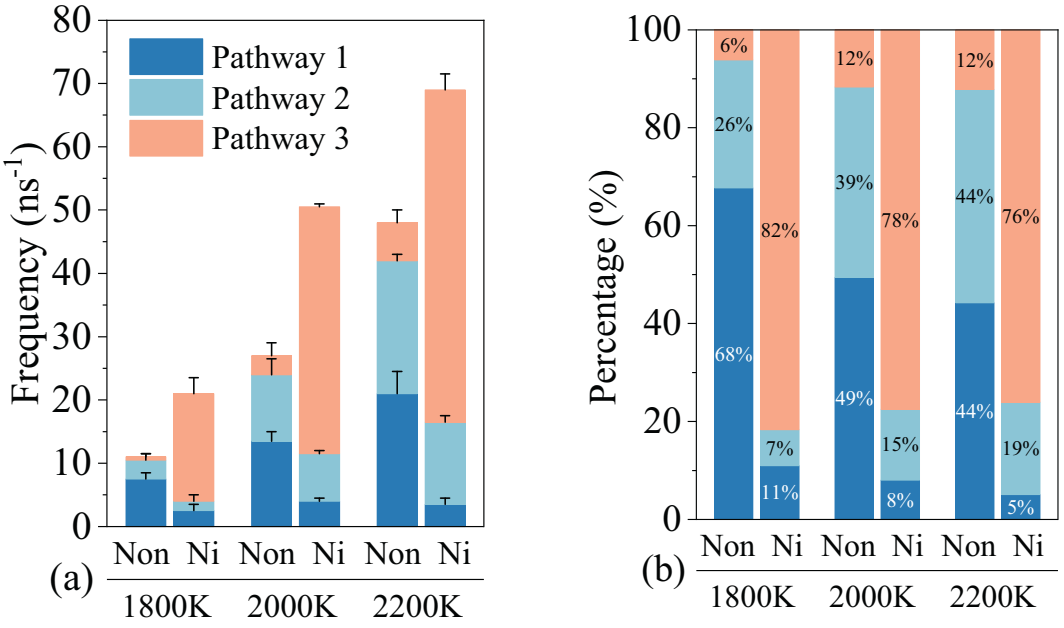

Fig. 6 – The (a) frequency and (b) proportion of H_2 generation pathways ①-③ in the absence and presence of Ni catalyst (cases S2 and S5).

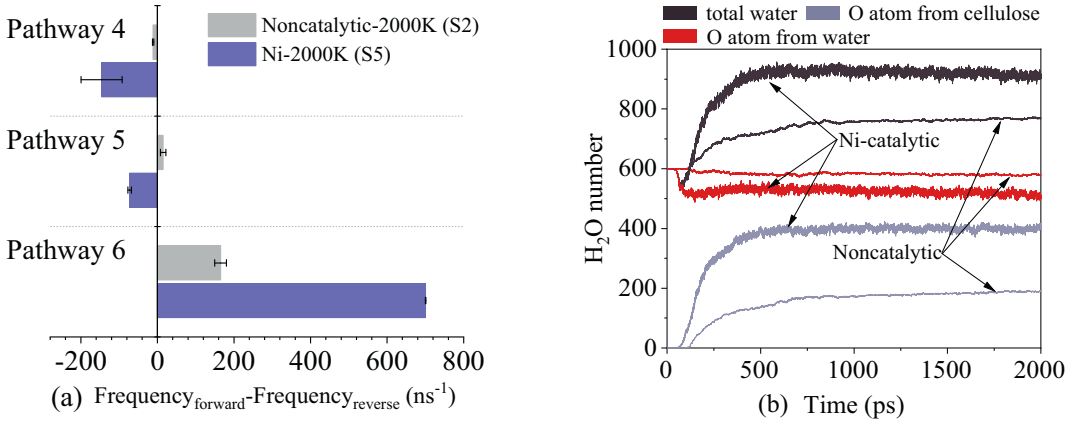

Fig. 7 – (a) The frequency difference of the forward and reverse reaction of pathways ④-⑥ in cases S2 and S5; (b) The total water molecule number and the source of O atom in water in cases S2 and S5.

Fig. 7(a) shows the frequency differences of forward and reverse reaction of pathway ④-⑥ in cases S2 and S5. It should be noted that the frequency of reverse reaction could be higher than that of the forward reaction, which is because the reactants involved in the reverse reaction could be produced from other reactions. For example, •OH could be generated from pathway ④, while it can also be produced from the cleavage of the C–O bond in cellulose (e.g., R – OH→R• + •OH). The cleavage of β-1,4 linkage and C–O bond in D-glucopyranose would produce R – O• that involved in the reverse reaction of pathway ⑤. The increase in these reactant concentrations would shift the reactions into the reverse direction. The results show that the H free radicals mainly come from the dehydrogenation reaction of H atoms connected to C atoms, e.g., pathway ⑥. The H radicals generated from pathway ⑥ increase with the addition of Ni, which can be attributed to the promotion effect of Ni on C–H bond cleavage [47].

Although the water splitting reaction would produce H radicals, the •OH generated from water and cellulose would consume H radicals to form water simultaneously. The frequency of pathway ④ reverse reaction is higher than that of the forward reaction, leading to an increase in water molecule number. This is due to the structural features of cellulose, which has a large number of hydroxy groups. The increase in •OH concentration shifts the reaction of pathway ④ to the reverse direction, especially with the addition of Ni catalyst, since Ni could promote the scission of C–O bonds to produce more •OH.

Experimental results suggested that one of the roles of water in SCWG is being a source of hydrogen and free radicals [3]. However, quantitative information on such effect is

difficult to obtain through experimental approaches. In ReaxFF MD simulation, the role of water in producing hydrogen and free radicals can be identified by tracing the evolution of the original water (the water that was added to the system in the initial stage). Fig. 7(b) indicates the total water molecule number and the source of O atom in water in cases S2 and S5. Although it was observed that the frequencies of forward and reverse reaction of pathway ④ are high, especially on Ni surface, only a small part of the original water split into H• and •OH in the end, as indicated by the red line in Fig. 7(b). The results indicate that only a limited number of H radicals produced from pathway ④ forward reaction could be the source of H_2 generation. Moreover, Ni could promote the splitting reaction of water, and the reduction of original water in the presence of Ni is more significant. The increased water in two cases is ascribed to the combination of H radicals and hydroxy groups dissociated from cellulose since the oxygen atom in increased water mainly comes from cellulose, as indicated by the violet line in Fig. 7(b). The increase of total water molecule number in Ni catalytic SCWG is more significant than in noncatalytic SCWG as Ni could promote the cleavage of C–O bond to produce more hydroxy groups. It can be deduced that water plays a limited role in providing H free radicals to produce H_2, while the hydrogen atoms in cellulose are the primary source of H_2 generation.

A schematic diagram of H_2 generation pathways during the noncatalytic and Ni-catalytic SCWG of cellulose is shown in Fig. 8. In the absence of a catalyst, H free radicals would be generated via dehydrogenation of cellulose, and a small amount of water would also be split into H free radicals and •OH. H radicals generate H_2 through pathways ①-③, where pathway ① plays a leading role, followed by pathway ②. In the presence of Ni catalyst, the decomposed molecular fragments and water would be adsorbed on the Ni surface, where the scission of the C–H and O–H bonds is enhanced to produce a large number of H radicals. H radicals undergo radical termination reactions to produce H_2 (pathway ③), which dominates the H_2 generation. Meanwhile, the generated •OH would consume H radicals to form water. In the absence of catalyst, mainly comes from pathway ②. Nevertheless, cellulose also produces some •OH on the Ni surface via the cleavage of C–O bonds when Ni is added. The •OH generated through serval pathways would consume a relatively large amount of H radicals, leading to an increase in H_2O molecule number. It can be found that the generation of H_2O is an H radical consumption process. The concentration of H radicals would increase if the number of •OH in the reacting system can be suppressed, thereby increasing the yield of H_2.

It can be seen in Fig. 5 that the yield of CO is enhanced at elevated temperature in the absence of a catalyst, which is consistent with the experimental results [48]. The elevated temperature would promote the cleavage of C–C bonds, thereby enhancing the yield of gaseous products. CO yield decreased significantly when the catalyst was added. Yoshida et al. [42] attributed the reduction of CO to the enhancement of water-gas shift reaction ($CO + H_2O \rightarrow CO_2 + H_2$), and the disproportionation of carbon monoxide adsorbed on the catalyst surface ($2CO \rightarrow CO_2 + C$). However, this study found that the molecular fragments produced by cellulose dissociation would be adsorbed on the catalyst surface [30]. The C–O bonds would be cracked under the catalytic effect of Ni, as shown in Fig. 9(a). Oxygen atoms that might be used to generate CO are prone to be detached from organic fragments to produce water by interacting with H radicals. It is demonstrated that the deoxygenation and dehydroxylation of organic fragments on Ni surface are the main reason for CO reduction.

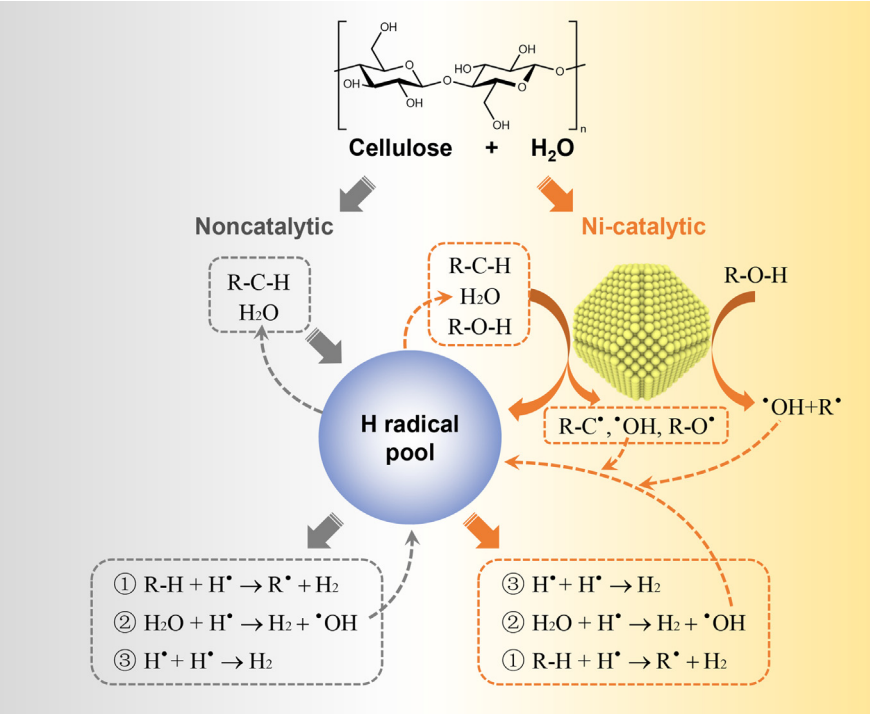

Fig. 8 – Schematic diagram of H_2 generation pathways during noncatalytic and Ni-catalytic SCWG of cellulose.

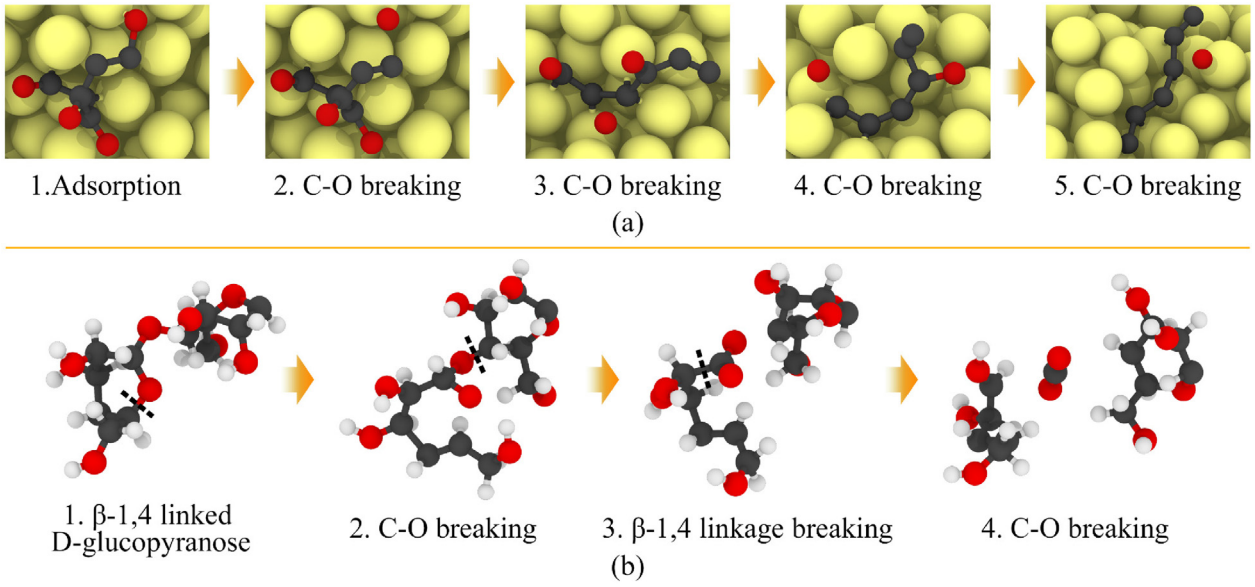

Fig. 9 – (a) The cleavage of C–O bonds on the Ni surface; (b) The primary generation process of CO_2. Dash lines represent the bond cleavage sites.

There was a slight change in the yield of CO_2 when the temperature increased, as shown in Fig. 5, which is ascribed to the structural features of cellulose. The carbon atom connected with two oxygen atoms is the primary source of CO_2, as illustrated in Fig. 9(b). There are a small number of β-1,4 linkage in cellulose; thus, the yield of CO_2 is lower than H_2 and CO [49]. Consequently, the effects of temperature and catalyst on CO_2 production are weaker than those on H_2 and CO.

The effect of C/W on gaseous product yield

Fig. 10 presents the yields of H_2, CO, and CO_2 under different C/W at 2000 K. The H_2 yield increases slightly with the increasing number of water molecules, which is consistent with experimental results [23]. Increasing the water molecule number favours the forward reaction of pathway ④, leading to an increase in H radical number, as shown in Fig. 11(a). In the presence of Ni catalyst, a large number of H radicals would be generated via water splitting and cellulose dehydrogenation reactions on the Ni surface. Then H radicals are continuously consumed to produce H_2 and H_2O. A high concentration of H radicals contributes to the formation of H_2.

Typically, water and small organic fragments would be adsorbed on metal catalyst [50], as shown in Fig. 11(b). It was observed that the addition of water occupies a part of the active sites on the catalyst surface, which weakens the adsorption capacity of the catalyst to organic fragments [23]. When most of the active sites of the Ni catalyst are occupied by water or hydroxyl group, the small dissociative fragments outside Ni surface will generate CO via the cleavage of C–C

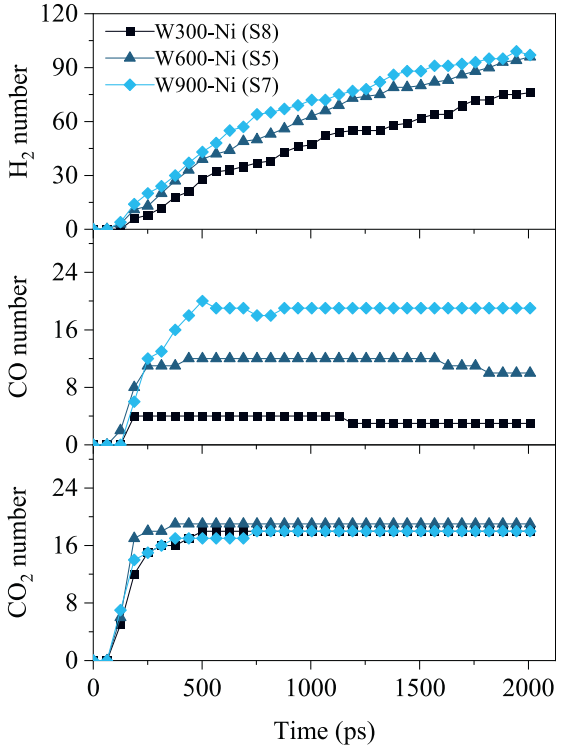

Fig. 10 – Time evolution of H_2, CO, and CO_2 yields under different C/W conditions during Ni-catalytic SCWG of cellulose (cases S8, S5, and S7).

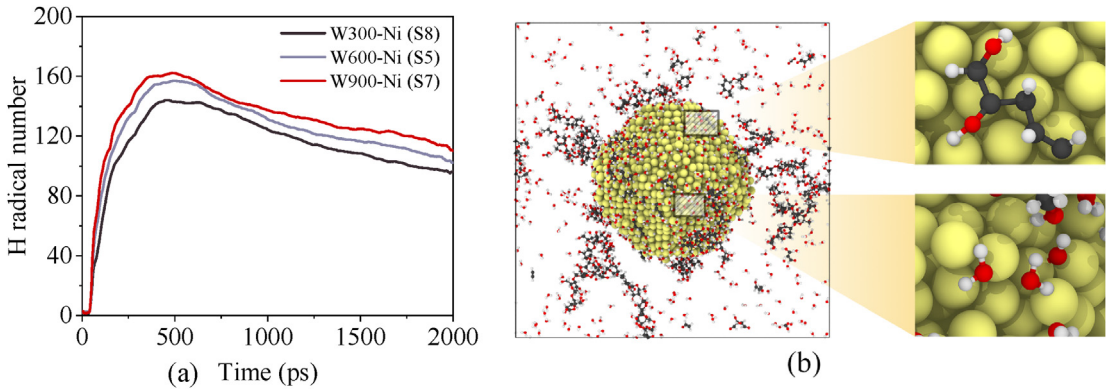

Fig. 11 – (a) Time evolution of H radical number under different C/W conditions; (b) Snapshots of surface conditions of Ni catalyst, where the adsorption of small organic fragments and water on Ni active sites are highlighted on the right.

bonds. Therefore, the yield of CO increases with the addition of water, as shown in Fig. 10. The influence of C/W on CO_2 production is negligible since CO_2 mainly comes from the carbon that is connected to the two oxygen atoms, and the production of CO_2 is relatively low as stated before.

Carbon deposition on Ni catalyst

Deactivation of catalysts is unavoidable in the catalytic SCWG reaction process. Carbon/coke deposition on catalyst surface is regarded as one main problem for the deactivation of Ni-based catalysts [51]. To investigate the carbon deposition and permeation behaviour in SCWG of cellulose, the carbon deposition and permeation on Ni surface under different temperatures and C/W were analysed. The block of NiNP was divided into three zones (inside the spherical shell) according to different radii, as illustrated in Fig. 12(a). Carbon deposition rate is determined by the number of carbon atoms in different zones. Fig. 12(b) shows carbon migration on the catalytic surface and in catalyst pores. There are a small number of carbon atoms in Zone 3 at 100 ps, and then the carbon atoms permeate into the inside of NiNP at 250 ps. The evolution of carbon number in different zones under varying temperatures is presented in Fig. 12(d). The results show that carbon atoms infiltrate into Ni over time, and there is no noticeable difference in the total number of carbon when reaching an equilibrium state. However, the difference in the deposition rates under varying temperatures is appreciable. A small number of carbon atoms can be detected in Zone 2 at 250 ps when the temperature is 1800 K. With the increase in temperature, carbon would reach Zone 2 at an earlier time, at around 150 ps. The time instants for carbon reaching Zone 1 at 1800 K, 2000 K, and 2200 K are around 375 ps, 180 ps, and 130 ps, respectively. The results indicate that the permeation rate of carbon increases with increasing temperature. Nevertheless, the number of carbon molecules at the equilibrium state in different zones is roughly the same, which suggests that temperature has a negligible impact on the degree of carbon permeation.

To uncover the carbon permeation mechanism on NiNP at different temperatures, the atomic order of Ni atoms was analysed. Steinhardt's bond orientational order parameters Q_l (where l can take an integer value between 0 and infinity) [52] were used to explore the local atomic environment. These order parameters are mathematically defined based on certain rotationally invariant combinations of spherical harmonics calculated between atoms and their nearest neighbours, providing information about local atom environments. Q_l has been used for various purposes, such as the structure identification of solid and liquid systems [53]. Commonly Q_6 is used in the identification of cubic lattice structure. All the particles in a perfect ordered structure have the same value of Q_6. As a results, Q_6 values can be used to determine whether an ordered structure is beginning to turn into a disordered structure. Therefore, Q_6 was adopted to characterise the atomic order of NiNP, which was built as a face-centred cubic lattice structure in this study. The magnitude of Q_6 is large when the Ni atoms are ordered and small when the Ni atoms are disordered.

Fig. 12(c) shows the sectional view of NiNP atomic Q_6 values at different times. The internal atoms of NiNP are in an ordered state in the initial stage and then in transition to a disordered state over time. The evolution of averaged atomic Q_6 of Ni atoms in different zones is presented in Fig. 12(e). The equilibrium Q_6 values decrease with increasing temperature. The position of atoms in the outermost shell (e.g., Zone 3) shifted first, and then the order degree of internal atoms decreased over time as heat was transferred to the interior region. The Q_6 values in Zone 2 and Zone 1 decreased more slowly under lower temperatures. For example, the Q_6 value in Zone 1 at 2200 K decreases significantly at around 125 ps, while the time instant for Q_6 dramatical reduction at 1800 K is about 310 ps. The decrease in Q_6 value represents that the crystal structure of NiNP is destroyed, and there is a relatively large displacement between Ni atoms. It is easier for carbon atoms to infiltrate into the NiNP when the displacement between Ni atoms becomes larger.

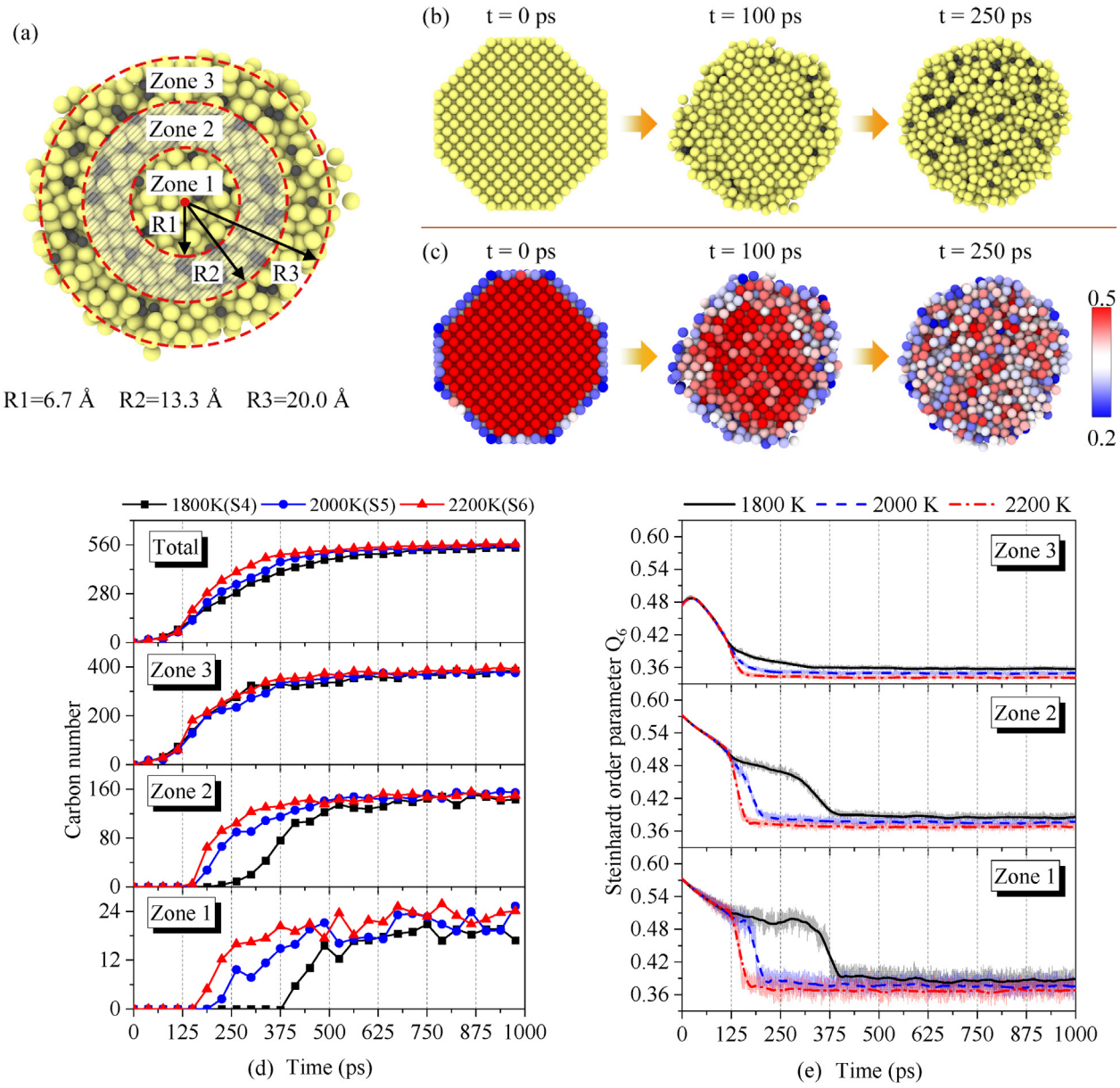

Fig. 12 – (a) The division method of NiNP in different zones; (b) The sectional view of the carbon migration process in NiNP; (c) The sectional view of atomic Q_6 values of NiNP; (d) The evolution of carbon number in different zones under varying temperatures; (e) The evolution of averaged atomic Q_6 values in different zones.

Fig. 13 shows the evolution of carbon numbers in different zones under varying C/W. The time that carbon reaches Zone 2 and Zone 1 is roughly the same under different C/W conditions, demonstrating that C/W has a negligible influence on carbon permeation on NiNP surface and in NiNP pores. Nevertheless, high C/W would inhibit the carbon deposition number on NiNP. The equilibrium carbon numbers in total and in different zones decrease with the increase in water molecule number. Wu and Liu [51] also reported that the increase of the steam to carbon ratio could favour carbon elimination during bio-oil gasification. The carbon elimination from the catalyst surface can be ascribed to the addition of water occupying the active sites on the catalyst surface, preventing the dissociative carbon atoms from attaching to NiNP.

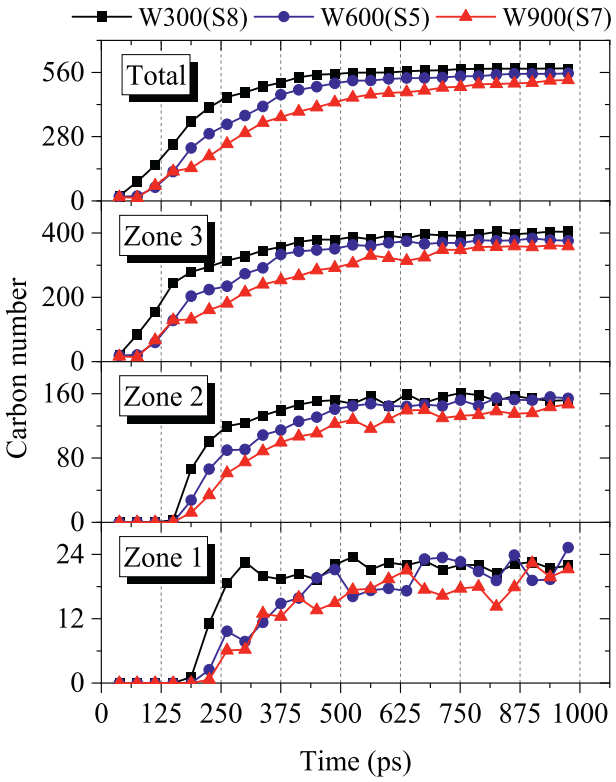

Fig. 13 – The evolution of carbon number in different zones under varying C/W.

Conclusions

In this study, Nickel catalysed gasification of cellulose in supercritical water is investigated by using reactive MD simulation. The depolymerisation and ring-opening process of cellulose, effects of Ni and C/W on gaseous product yield, and carbon deposition behaviour on Ni catalyst were investigated. This study provides detailed information on Ni-catalysed cellulose SCWG at an atomic level.

Calculated activation energies show that Ni can decrease the activation energy of C–C and C–O bond cleavage, promoting cellulose depolymerisation and ring-opening process. Cellulose could be gasified at a lower temperature with the addition of Ni. The activation energy reduction of C–O is more significant than that of C–C bonds under the effect of Ni.

The H_2, CO, and CO_2 yields increase with increasing temperature. H_2 yield increases significantly in the presence of Ni due to the large number of hydrogen free radicals generated by the cleavage of C–H and O–H bonds on the surface of NiNP. H radicals can not only interact with each other to produce H_2 but also interact with H atoms on water and cellulose to generate H_2. The $^{\bullet}OH$ generated would consume H radicals, leading to an increase in H_2O number. The concentration of H radicals would increase if the number of $^{\bullet}OH$ in the reacting system can be suppressed, thereby increasing the yield of H_2. Simulation results show that water plays a limited role in providing H free radicals to produce H_2, the hydrogen atoms in cellulose are the primary source of H_2 generation. The cellulose cracking fragments would be adsorbed on the NiNP surface, where these fragments undergo deoxygenation and dehydroxylation reactions, leading to a reduction of CO and CO_2 yields. The addition of water will occupy the active sites on Ni surface, reducing the probability of molecular fragments attaching to the Ni surface. The small dissociative fragments outside Ni surface tend to generate more CO.

The carbon deposition on the NiNP surface results in the deactivation of the catalyst. Due to the movement of Ni atoms at high temperature, the adsorbed carbon would infiltrate into the NiNP. Results suggest that carbon permeation rate increases with increasing temperature as the relative displacement of Ni atoms would be increased under higher temperatures. The increase in water mass fraction can favour carbon elimination from the catalyst surface because water would occupy the active sites on the NiNP surface, resulting in the failure of carbon adsorption. This study elucidated the detailed mechanism of Ni-catalysed cellulose SCWG from the molecular point of view, providing a basis for further biomass utilisation and cost reduction.

Declaration of competing interest

The authors declare that they have no known competing financial interests or personal relationships that could have appeared to influence the work reported in this paper.

Acknowledgements

Supercomputing time on ARCHER is provided by the "UK Consortium on Mesoscale Engineering Sciences (UKCOMES)" under the UK Engineering and Physical Sciences Research Council Grant No. EP/R029598/1. This work made use of computational support by CoSeC, the Computational Science Centre for Research Communities, through UKCOMES.

REFERENCES

[1] Okolie JA, Rana R, Nanda S, Dalai AK, Kozinski JA. Supercritical water gasification of biomass: a state-of-the-art review of process parameters, reaction mechanisms and catalysis. Sustain Energy Fuels 2019;3(3):578–98.
[2] Yoshida Y, Dowaki K, Matsumura Y, Matsuhashi R, Li D, Ishitani H, et al. Comprehensive comparison of efficiency and CO_2 emissions between biomass energy conversion technologies-position of supercritical water gasification in biomass technologies. Biomass Bioenergy 2003;25(3):257–72.
[3] Hu Y, Gong M, Xing X, Wang H, Zeng Y, Xu CC. Supercritical water gasification of biomass model compounds: a review. Renew Sustain Energy Rev 2020;118:109529.
[4] Shrotri A, Kobayashi H, Fukuoka A. Cellulose depolymerization over heterogeneous catalysts. Accounts Chem Res 2018;51(3):761–8.
[5] Lee CS, Conradie AV, Lester E. Review of supercritical water gasification with lignocellulosic real biomass as the feedstocks: process parameters, biomass composition, catalyst development, reactor design and its challenges. Chem Eng J 2021;415:128837.

[6] Hassan NS, Jalil AA, Vo DVN, Nabgan W. An overview on the efficiency of biohydrogen production from cellulose. Biomass Conversion and Biorefinery; 2020.
[7] Yakaboylu O, Harinck J, Smit K, De Jong W. Supercritical water gasification of biomass: a literature and technology overview. Energies 2015;8(2):859–94.
[8] Hu Y, Gong M, Feng S, Xu C, Bassi A. A review of recent developments of pre-treatment technologies and hydrothermal liquefaction of microalgae for bio-crude oil production. Renew Sustain Energy Rev 2019;101:476–92.
[9] Guo Y, Wang SZ, Xu DH, Gong YM, Ma HH, Tang XY. Review of catalytic supercritical water gasification for hydrogen production from biomass. Renew Sustain Energy Rev 2010;14(1):334–43.
[10] Ren J, Cao J-P, Zhao X-Y, Yang F-L, Wei X-Y. Recent advances in syngas production from biomass catalytic gasification: a critical review on reactors, catalysts, catalytic mechanisms and mathematical models. Renew Sustain Energy Rev 2019;116:109426.
[11] Zeng X, Fang M, Lv T, Tian J, Xia Z, Cen J, et al. Enhanced hydrogen production by the catalytic alkaline thermal gasification of cellulose with Ni/Fe dual-functional CaO based catalysts. Int J Hydrogen Energy 2021;46(65):32783–99.
[12] Lee I-G, Ihm S-K. Catalytic gasification of glucose over Ni/activated charcoal in supercritical water. Ind Eng Chem Res 2009;48(3):1435–42.
[13] Grams J, Potrzebowska N, Goscianska J, Michalkiewicz B, Ruppert AM. Mesoporous silicas as supports for Ni catalyst used in cellulose conversion to hydrogen rich gas. Int J Hydrogen Energy 2016;41(20):8656–67.
[14] Ruppert AM, Niewiadomski M, Grams J, Kwapiński W. Optimization of Ni/ZrO_2 catalytic performance in thermochemical cellulose conversion for enhanced hydrogen production. Appl Catal B Environ 2014;145:85–90.
[15] Świerczyński D, Libs S, Courson C, Kiennemann A. Steam reforming of tar from a biomass gasification process over Ni/olivine catalyst using toluene as a model compound. Appl Catal B Environ 2007;74(3–4):211–22.
[16] Kumar A, Reddy SN. Subcritical and supercritical water in-situ gasification of metal (Ni/Ru/Fe) impregnated banana pseudo-stem for hydrogen rich fuel gas mixture. Int J Hydrogen Energy 2020;45(36):18348–62.
[17] Li H, Xu B, Jin H, Luo K, Fan J. Molecular dynamics investigation on the lignin gasification in supercritical water. Fuel Process Technol 2019;192:203–9.
[18] Liu XY, Wang T, Chu JC, He MG, Li QB, Zhang Y. Understanding lignin gasification in supercritical water using reactive molecular dynamics simulations. Renew Energy 2020;161:858–66.
[19] Ponnuchamy V, Sandak J, Sandak A. Revealing of supercritical water gasification process of lignin by reactive force field molecular dynamics simulations. Processes 2021;9(4):714.
[20] Wang T, Liu X, Huang S, Waheed A, He M. Modelling co-gasification of plastic waste and lignin in supercritical water using reactive molecular dynamics simulations. Int J Hydrogen Energy 2022;47(49):21060–6.
[21] Zhang Y-M, Li J-L, Wang J-P, Yang X-S, Wang B-Z. ReaxFF MDSs-based studies on gasification of glucose in supercritical water under microwave heating. Int J Hydrogen Energy 2016;41(31):13390–8.
[22] Monti S, Srifa P, Kumaniaev I, Samec JSM. ReaxFF simulations of lignin fragmentation on a Palladium-based heterogeneous catalyst in methanol–water solution. J Phys Chem Lett 2018;9(18):5233–9.
[23] Wang T, Liu X, Liu H, He M. Synergistic effect of supercritical water and nano-catalyst on lignin gasification. Int J Hydrogen Energy 2021;46(70):34626–37.
[24] Zhang H, Chen F, Zhang J, Han Y. Supercritical water gasification of fuel gas production from waste lignin: the effect mechanism of different oxidized iron-based catalysts. Int J Hydrogen Energy 2021;46(59):30288–99.
[25] Han Y, Chen F, Ma T, Gong H, Al-Shwafy KWA, Li W, et al. Size effect of a Ni nanocatalyst on supercritical water gasification of lignin by reactive molecular dynamics simulations. Ind Eng Chem Res 2019;58(51):23014–24.
[26] Saha B, Patra AS, Mukherjee AK, Paul I. Interaction and thermal stability of carboxymethyl cellulose on α-Fe_2O_3 (001) surface: ReaxFF molecular dynamics simulations study. J Mol Graph Model 2021;102:107787.
[27] van Duin ACT, Dasgupta S, Lorant F, Goddard WA. ReaxFF: a reactive force field for hydrocarbons. J Phys Chem 2001;105(41):9396–409.
[28] Mueller JE, van Duin ACT, Goddard WA. Application of the ReaxFF reactive force field to reactive dynamics of hydrocarbon chemisorption and decomposition. J Phys Chem C 2010;114(12):5675–85.
[29] Mueller JE, van Duin ACT, Goddard WA. Development and validation of ReaxFF reactive force field for hydrocarbon chemistry catalyzed by Nickel. J Phys Chem C 2010;114(11):4939–49.
[30] Chen C, Volpe R, Jiang X. A molecular investigation on lignin thermochemical conversion and carbonaceous organics deposition induced catalyst deactivation. Appl Energy 2021;302:117557.
[31] BIOVIA. Materials Studio. San Diego: Dassault Systèmes.
[32] Chatzigoulas A, Karathanou K, Dellis D, Cournia Z. Nanocrystal: a web-based crystallographic tool for the construction of nanoparticles based on their crystal habit. J Chem Inf Model 2018;58(12):2380–6.
[33] So/rensen MR, Voter AF. Temperature-accelerated dynamics for simulation of infrequent events. J Chem Phys 2000;112(21):9599–606.
[34] Han Y, Ma T, Chen F, Li W, Zhang J. Supercritical water gasification of naphthalene over iron oxide catalyst: a ReaxFF molecular dynamics study. Int J Hydrogen Energy 2019;44(57):30486–98.
[35] Salmon E, van Duin ACT, Lorant F, Marquaire P-M, Goddard WA. Early maturation processes in coal. Part 2: reactive dynamics simulations using the ReaxFF reactive force field on Morwell Brown coal structures. Org Geochem 2009;40(12):1195–209.
[36] Martínez L, Andrade R, Birgin EG, Martínez JM. PACKMOL: a package for building initial configurations for molecular dynamics simulations. J Comput Chem 2009;30(13):2157–64.
[37] Aktulga HM, Fogarty JC, Pandit SA, Grama AY. Parallel reactive molecular dynamics: nnumerical methods and algorithmic techniques. Parallel Comput 2012;38(4–5):245–59.
[38] Thompson AP, Aktulga HM, Berger R, Bolintineanu DS, Brown WM, Crozier PS, et al. Lammps - a flexible simulation tool for particle-based materials modeling at the atomic, meso, and continuum scales. Comput Phys Commun 2022;271:108171.
[39] Kabyemela BM, Adschiri T, Malaluan RM, Arai K. Glucose and fructose decomposition in subcritical and supercritical water: detailed reaction pathway, mechanisms, and kinetics. Ind Eng Chem Res 1999;38(8):2888–95.
[40] Si T, Huang K, Lin Y, Gu M. ReaxFF study on the effect of CaO on cellulose pyrolysis. Energy Fuels 2019;33(11):11067–77.
[41] Chen C, Zhao L, Wang J, Lin S. Reactive molecular dynamics simulations of biomass pyrolysis and combustion under various oxidative and humidity environments. Ind Eng Chem Res 2017;56(43):12276–88.
[42] Yoshida T, Oshima Y, Matsumura Y. Gasification of biomass model compounds and real biomass in supercritical water. Biomass Bioenergy 2004;26(1):71–8.

[43] Ding N, Azargohar R, Dalai AK, Kozinski JA. Catalytic gasification of cellulose and pinewood to H_2 in supercritical water. Fuel 2014;118:416–25.
[44] Peters W, Seidel A, Herzog S, Bösmann A, Schwieger W, Wasserscheid P. Macrokinetic effects in perhydro-N-ethylcarbazole dehydrogenation and H_2productivity optimization by using egg-shell catalysts. Energy Environ Sci 2015;8(10):3013–21.
[45] Bühler W, Dinjus E, Ederer HJ, Kruse A, Mas C. Ionic reactions and pyrolysis of glycerol as competing reaction pathways in near- and supercritical water. J Supercrit Fluids 2002;22(1):37–53.
[46] Muroya Y, Yamashita S, Lertnaisat P, Sanguanmith S, Meesungnoen J, Jay-Gerin JP, et al. Rate constant for the $H + H_2O \rightarrow \dot{O}H + H_2$ reaction at elevated temperatures measured by pulse radiolysis. Phys Chem Chem Phys 2017;19(45):30834–41.
[47] Che F, Ha S, McEwen JS. Catalytic reaction rates controlled by metal oxidation state: C–H bond cleavage in methane over nickel-based catalysts. Angew Chem 2017;129(13):3611–5.
[48] Shen DK, Gu S. The mechanism for thermal decomposition of cellulose and its main products. Bioresour Technol 2009;100(24):6496–504.
[49] Wu C, Wang Z, Huang J, Williams PT. Pyrolysis/gasification of cellulose, hemicellulose and lignin for hydrogen production in the presence of various nickel-based catalysts. Fuel 2013;106:697–706.
[50] Soria FA, Di Valentin C. Reactive molecular dynamics simulations of hydration shells surrounding spherical TiO_2 nanoparticles: implications for proton-transfer reactions. Nanoscale 2021;13(7):4151–66.
[51] Wu C, Liu R. Carbon deposition behavior in steam reforming of bio-oil model compound for hydrogen production. Int J Hydrogen Energy 2010;35(14):7386–98.
[52] Steinhardt PJ, Nelson DR, Ronchetti M. Bond-orientational order in liquids and glasses. Phys Rev B 1983;28(2):784–805.
[53] Zhao J, Song W-X, Xin T, Song Z. Rules of hierarchical melt and coordinate bond to design crystallization in doped phase change materials. Nat Commun 2021;12(1).